Published in "Nature Materials 8: 315-319, 2009"
which should be cited to refer to this work.

Giant superconductivity-induced modulation of the ferromagnetic magnetization in a cuprate–manganite superlattice

J. Hoppler[1,2], J. Stahn[2]*, Ch. Niedermayer[2], V. K. Malik[1], H. Bouyanfif[1†], A. J. Drew[1†], M. Rössle[1], A. Buzdin[3], G. Cristiani[4], H.-U. Habermeier[4], B. Keimer[4] and C. Bernhard[1]*

Artificial multilayers offer unique opportunities for combining materials with antagonistic orders such as superconductivity and ferromagnetism and thus to realize novel quantum states[1,2]. In particular, oxide multilayers enable the utilization of the high superconducting transition temperature of the cuprates and the versatile magnetic properties of the colossal-magnetoresistance manganites[3–6]. However, apart from exploratory work[7–10], the in-depth investigation of their unusual properties has only just begun[11–15]. Here we present neutron reflectometry measurements of a [$Y_{0.6}Pr_{0.4}Ba_2Cu_3O_7$ (10 nm)/$La_{2/3}Ca_{1/3}MnO_3$ (10 nm)]$_{10}$ superlattice, which reveal a surprisingly large superconductivity-induced modulation of the vertical ferromagnetic magnetization profile. Most surprisingly, this modulation seems to involve the density rather than the orientation of the magnetization and is highly susceptible to the strain, which is transmitted from the $SrTiO_3$ substrate. We outline a possible explanation of this unusual superconductivity-induced phenomenon in terms of a phase separation between ferromagnetic and non-ferromagnetic nanodomains in the $La_{2/3}Ca_{1/3}MnO_3$ layers.

The competition between superconductivity and ferromagnetism is one of the most fascinating and challenging topics in modern solid-state physics[16]. Prominent features are the so-called π-state, where the superconducting (SC) order parameter changes sign across the ferromagnetic (FM) layer, and SC–FM giant-magnetoresistance devices and subsequent spin filters[1,2]. These have been realized in of conventional low-T_c superconductors and ferromagnets which operate only at low temperatures. In comparison, the in-depth investigation of multilayers from oxide SC and FM materials has only recently begun[11–15]. This is in spite of their obvious advantages, like the high T_c values of the cuprates or the versatile magnetic properties of the manganites[3–6], which can be strongly modified by weak perturbations such as an external magnetic field[17] or possibly even by the proximity to SC layers.

Here we present evidence for the latter possibility from neutron reflectometry measurements on a [$Y_{0.6}Pr_{0.4}Ba_2Cu_3O_7$ (10 nm)/$La_{2/3}Ca_{1/3}MnO_3$(10 nm)]$_{10}$ (YPr-123/LCMO) superlattice grown on a 100-oriented $SrTiO_3$ (STO) substrate. Specifically, we find that the onset of superconductivity gives rise to a giant modulation of the FM magnetization profile, which seems to involve a change of the

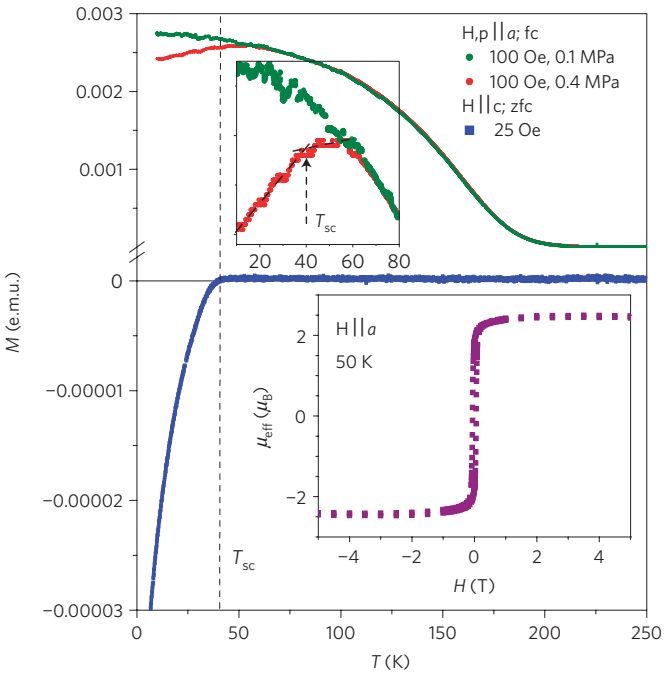

Figure 1 | Temperature- and pressure-dependent magnetization data. Magnetization data of the [$Y_{0.6}Pr_{0.4}Ba_2Cu_3O_7$ (10 nm)/$La_{2/3}Ca_{1/3}MnO_3$ (10 nm)]$_{10}$ superlattice showing the FM transition at $T_{Curie} \approx 190$ K and the SC one at $T_{sc} \approx 40$ K. The zero-field-cooled (zfc) data (blue symbols) show a clear onset of the diamagnetic signal below $T_{sc} \approx 40$ K. They were taken on a small piece that was cut from the sample, the magnetic field was perpendicular to the layers and no external pressure was applied. The field-cooled (fc) data were taken on the larger piece that was used for the neutron measurements. The magnetic field and the uniaxial pressure of 0.1 MPa (green symbols) and 0.4 MPa (red symbols) were applied parallel to the *a* axis of the $SrTiO_3$ substrate. A pressure dependence of the fc magnetization becomes noticeable below 60 K. Upper inset: Magnification of the low-temperature range of the fc magnetization data, showing the pressure-induced changes. Lower inset: Magnetization loop at $T = 50$ K, revealing a very soft FM behaviour and a saturation moment of about 2.4 μ_B per Mn ion.

[1]Physics Department and Fribourg Center for Nanomaterials (FriMat), Fribourg University, Chemin du Musée 3, CH-1700 Fribourg, Switzerland, [2]Laboratory for Neutron Scattering, ETH Zurich & Paul Scherrer Institut, CH-5232 Villigen PSI, Switzerland, [3]Condensed Matter Theory Group, CPMOH, UMR 5798, Université Bordeaux I, F-33405 Talence Cedex, France, [4]Max-Planck-Institut für Festkörperforschung, Heisenbergstrasse 1, D-70569 Stuttgart, Germany. †Present addresses: Laboratoire de Physique de la Matière Condensée, Université de Picadie Jules Verne, 80000 Amiens, France (H.B.); Queen Mary University of London, Department of Physics, Mile End Road, London, E1 4NS, UK (A.J.D.). *e-mail: Jochen.stahn@psi.ch; christian.bernhard@unifr.ch.

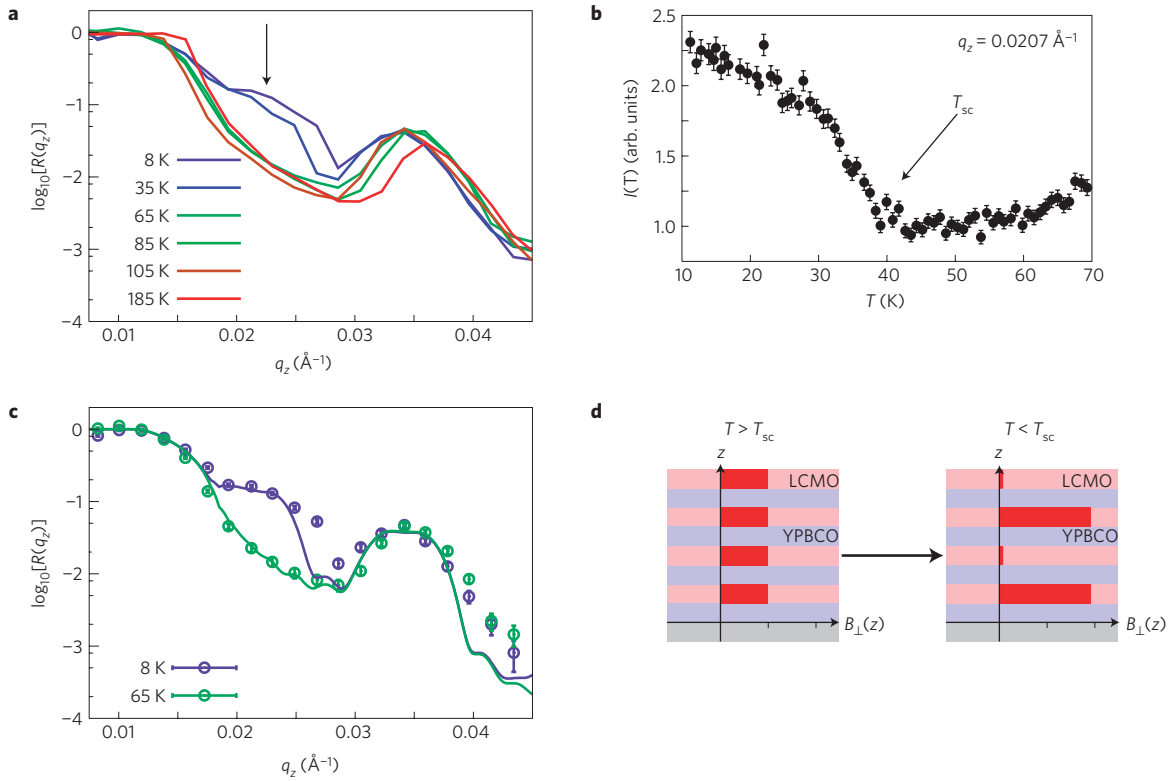

Figure 2 | Unpolarized neutron reflectivity spectra and their modelling. a, Temperature dependence of the unpolarized specular neutron reflectivity curves of a $[Y_{0.6}Pr_{0.4}Ba_2Cu_3O_7$ (10 nm)/$La_{2/3}Ca_{1/3}MnO_3$ (10 nm)$]_{10}$ superlattice as measured with the in-plane component of the neutron *k* vector along the *a* axis, corresponding to the (100) direction of the STO substrate. The arrow marks the position of the superconductivity-induced half-order superlattice Bragg peak. **b**, Detailed temperature evolution of the intensity at $q_z = 0.0207$ Å^{-1}, which confirms that the new Bragg peak develops right below $T_{sc} = 40$ K and thus is indeed related to a superconductivity-induced magnetic phenomenon. **c**, Theoretical simulations (solid lines) compared with the experimental spectra at 65 and 8 K. **d**, Sketch of the superlattice and the block-like magnetic potentials that were used for the simulations as shown in **c**. The length of the solid red bars is proportional to the FM magnetization of the $La_{2/3}Ca_{1/3}MnO_3$ layers. Error bars show the statistical errors.

density of the FM magnetization rather than its direction. We also show that this unusual superconductivity-induced phenomenon is extremely sensitive to the strain that is transmitted from the STO substrate.

The d.c. magnetization data shown in Fig. 1 establish that our superlattice has an SC transition temperature of $T_{sc} \approx 40$ K and a Curie temperature of $T_{Curie} \approx 190$ K. The hysteresis loop in the lower inset confirms a very soft FM behaviour and yields a saturation moment of about 2.4 μ_B per Mn ion at 50 K. Rather remarkable are the field-cooled (fc) magnetization data, which reveal an interesting pressure dependence that sets in below 60 K. This onset coincides with a structural transition of the STO substrate, which is accompanied by the formation of micrometre-sized, strongly anisotropic domains that give rise to a tilting of the surface of up to 0.5°. Synchrotron X-ray[18] and neutron reflectometry measurements (see below) show that this tilting persists throughout the entire superlattice. The pressure-induced alignment of these structural domains apparently has a clear impact on the magnetic properties of our superlattice. It gives rise to sizeable changes in the fc magnetization data below 60 K and a small slope change near T_{sc}.

The latter superconductivity-induced effect is born out more clearly in the neutron reflectometry data of Figs 2–4, which resolve the corresponding changes of the vertical profile of the superlattice magnetization density. The sample was mounted here under uniaxial pressure by clamping it with spring-loaded screws on the cold finger of a cryostat. A sketch of the experimental set-up is given in Supplementary Fig. S1. The unpolarized specular neutron reflectometry spectra in Fig. 2a highlight that the onset of superconductivity gives rise to some truly remarkable changes in the vertical profile of the in-plane component of the FM magnetization. Notably, a new, strong peak develops near $q_z = 0.0207$ Å^{-1} close to the position of the half-order superlattice Bragg peak. Figure 2b details the T evolution of the intensity at $q_z = 0.0207$ Å^{-1} and confirms that the new fractional-order Bragg peak develops right below $T_{sc} \approx 40$ K. Its sheer magnitude suggests that the in-plane component of the FM magnetization must undergo some rather large superconductivity-induced modulation with a period that is nearly doubled when compared with the structural one.

In Fig. 2c,d we show that the spectra can be reasonably well reproduced with a model of block-like profiles of magnetic potentials in the LCMO layers. At $T > T_{sc}$ our simple model provides a very good fit to the data and thus yields a reliable estimate of the magnetic moment per Mn ion of $\mu \approx 2.1\,\mu_B$ (flux density $B = 0.44$ T). At $T < T_{sc}$ we obtain a large double-period modulation with an average FM magnetization and modulation amplitude amounting to $\mu \approx 2.1\,\mu_B$ (flux density $B = 0.44$ T) and $\Delta\mu \approx 1.9\,\mu_B$ ($\Delta B = 0.40$ T), respectively. The maximum value of $\mu^{max} \approx 4\,\mu_B$ is indeed close to the 3.7 μ_B per Mn of bulk LCMO (refs 4,19), which implies that the modulation amplitude acquires its largest possible value. It is the more surprising that the average magnetization of the entire superlattice remains almost unaffected by these drastic changes of the magnetization of the individual LCMO layers. This is evident from the T evolution of the first-order Bragg peak of the neutron data in Figs 2a and 3, as well as from the d.c. magnetization data in Fig. 1, where only very small changes are observed. The observation of this giant superconductivity-induced double-period modulation of the FM magnetization and the discussion of its possible origin is the main subject of the present letter. Accordingly,

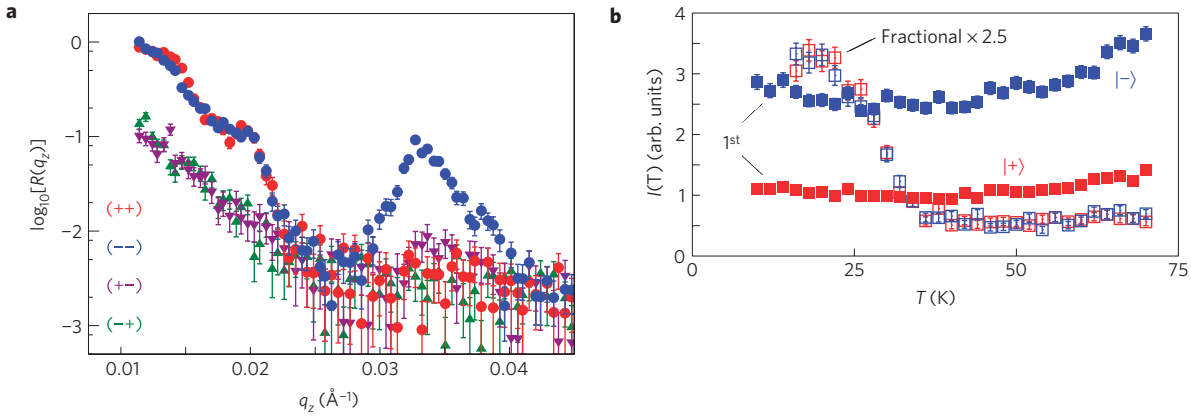

Figure 3 | Polarized neutron reflectometry spectra and temperature dependence of the fractional-order- and first-order superlattice Bragg peaks. **a**, Representative polarized specular reflectivity curves of the $[Y_{0.6}Pr_{0.4}Ba_2Cu_3O_7$ (10 nm)/$La_{2/3}Ca_{1/3}MnO_3$ (10 nm)$]_{10}$ superlattice as measured along the *a* direction. Circles show the non-spin-flip signals (R^{++} and R^{--}) and triangles show the extremely weak spin-flip signal (R^{+-} and R^{-+}). The arrow marks the position of the fractional-order superlattice Bragg peak. The strong peak centred around $q_z \approx 0.032$ Å^{-1} corresponds to the first-order Bragg peak. **b**, Temperature dependence of the intensity at the positions of the first-order (solid symbols) and the fractional-order (open symbols) superlattice Bragg peaks for the non-spin-flip channels. The latter have been up-scaled by a factor of 2.5. Error bars show the statistical errors.

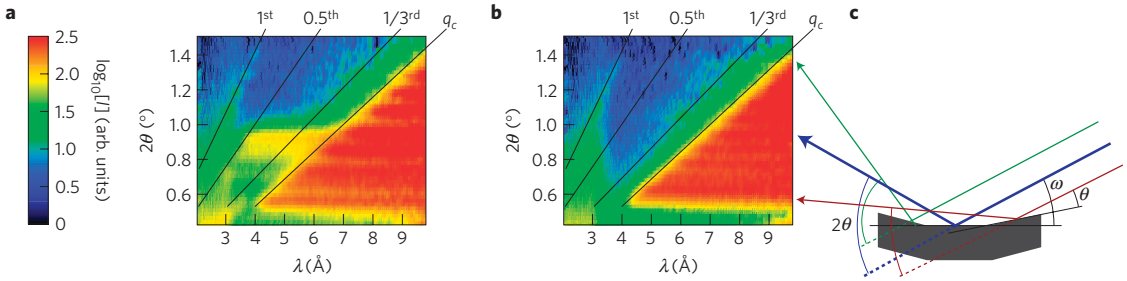

Figure 4 | Influence of the uniaxial pressure on the fractional-order Bragg peak and the structural and magnetic domains. a,**b**, Off-specular neutron reflectivity data in the non-spin-flip (R^{--}) channel that were collected with an area detector in time-of-flight mode at $T = 8$ K with the sample mounted under different uniaxial pressures of 0.4 and 0.1 MPa, respectively, along the *a* axis corresponding to the (100) direction of the STO substrate. The signals from the differently oriented facets of the sample surface appear here on straight horizontal lines at different values of 2θ, where θ corresponds to the angle of incidence of the neutron beam with respect to the facets (**c**). The relationship between the vertical momentum transfer, q_z, and the neutron wavelength, λ, is $q_z = 4\pi\sin\theta/\lambda$. The reflection edge at q_c and the third-, half- and first-order Bragg peaks thus fall on lines through the origin of the 2θ–λ plot, as indicated by the black lines. At 0.4 MPa (**a**) a strong fractional-order superlattice Bragg peak appears for several (but not all of the) facets. At 0.1 MPa (**b**) and above T_{sc} (not shown here) this fractional-order Bragg peak is entirely absent. The maps also reveal a sizeable pressure dependence of the facet formation and ordering. This is clearly seen for the data in the region of total reflection at $q_z < q_c$, where the modulation of the intensity along the 2θ axis is more pronounced at 0.4 MPa (**a**) than at 0.1 MPa (**b**).

we refrain from attempts to further improve the quality of the fits, for example by allowing for a variation of the magnetic moment within the LCMO layers. We also do not consider the previously observed proximity-induced FM moment in the SC layer[12,15], SC vortices or other kinds of unconventional SC currents, which can yield only minor contributions to the observed modulation.

Instead, we return to the essential question about the nature of the superconductivity-induced modulation of the in-plane FM moment. Naturally, we would expect that it is caused by a spin-canting effect, that is, it should involve a spiral magnetic state. However, our data are not compatible with such a scenario. An in-plane spin canting is firmly excluded by the polarized neutron data in Fig. 3, which show that the spin-flip signal, as a direct measure of an in-plane component in the direction perpendicular to the external field (see Supplementary Information), remains very weak. An out-of-plane canting, even though our neutron measurements do not directly probe the out-of-plane component, is also at variance with the combined neutron and d.c. magnetization data, which suggest that the moments are essentially parallel to the layers. In the normal state this is evident from the good agreement between the in-plane component of 2.1 μ_B as probed by the neutrons at 0.01 T and the total saturation moment of about 2.4 μ_B as derived from magnetization in Fig. 1. Accordingly, any out-of-plane canting in the SC state would only reduce the in-plane component; certainly, it could not give rise to the observed large increase of the maximal value.

Accordingly, our data are suggestive of a giant superconductivity-induced modulation of the magnitude of the FM magnetization in the LCMO layers. This can be energetically favourable only if there is a 'cheap way' of changing the magnetization density. Although this is not the case for ordinary FM materials, we argue that it may be possible for the present LCMO thanks to its versatile electromagnetic properties[3–6]. It is meanwhile well established that the manganites are very susceptible to phase segregation into nanodomains of either a double-exchange-induced FM metallic phase or a Jahn–Teller-stabilized paramagnetic or antiferromagnetic insulating phase[5,6]. The respective volume fractions and thus the average FM moment can indeed be strongly modified by relatively weak perturbations. For example, it has been demonstrated that moderate external magnetic fields can trigger a transition from an insulating and antiferromagnetic state to a metallic and FM one[17]. In analogy, it seems feasible that the proximity coupling to the SC layers can give rise to similarly dramatic changes in the FM magnetization density.

However, the required balance between the competing interactions in LCMO should be highly susceptible to the lattice strain. We find indeed that the superconductivity-induced anomaly strongly depends on the pressure that is applied to the substrate and the subsequent rearrangement of the structural domains. This is shown in Fig. 4, which details neutron reflectometry maps where the sample was mounted under well controlled uniaxial pressures of (a) 0.4 MPa and (b) 0.1 MPa. Most importantly, the fractional-order Bragg peak occurs here only at 0.4 MPa and is entirely absent at 0.1 MPa. As sketched in Fig. 4c, the reflection signals from the differently tilted micrometre-sized domains appear in these maps on horizontal lines that are spread along the 2Θ axis, where Θ is the angle between the incident neutron beam and the domain surfaces. Accordingly, the map at 0.4 MPa reveals that the fractional-order Bragg peak occurs for only some of the structural domains. Furthermore, these maps directly show that the uniaxial pressure gives rise to a rearrangement of the structural domains. This is best seen in the region of total reflection for $q_z < q_c$, where the contrast between the domains is noticeably stronger at 0.4 MPa than at 0.1 MPa. Finally, as detailed in Supplementary Fig. S4, the full map enables us to firmly exclude the possibility that the peak at the position of the fractional-order Bragg peak arises from small-angle scattering due to structural domains within the STO substrate.

The extreme strain dependence is also manifested in Supplementary Figs S5–S7, which shows that the occurrence of the fractional-order Bragg peak depends on the orientation of the applied pressure and the magnetic field with respect to the anisotropic domains, and that its position can be shifted depending on the details of the sample mounting. Overall, our data yield clear evidence that the ordering of the structural domains, which can be influenced by a relatively weak external pressure, is setting the stage for the giant superconductivity-induced modulation of the magnetization density in the LCMO layers.

We conclude with some interesting unresolved issues. The first one concerns the question of how the onset of SC in the YPr-123 layers can give rise to such a large modulation of the FM magnetization density. One possible explanation is in terms of the magnetic pair-breaking effects that arise from the coupling of the Cooper pairs with the magnetic exchange field, h, at the SC–FM interfaces. It was previously shown[20] that the related suppression of the SC condensation energy, dE^{cond}, scales like $dE^{\mathrm{cond}} \sim -h^2$, such that the gain in condensation energy at the interfaces with reduced h outweighs the losses at the interfaces with increased h. In contrast to ref. 20, where the thickness of the SC layer, d_s, was assumed to be short with respect to the SC coherence length, ξ_s, for our case we have the situation of $d_s > 2\xi_s$. Nevertheless, by simply replacing d_s with ξ_s in the calculations, to take into account that the pair breaking occurs only within a layer of thickness ξ_s near the interface, one also finds that the suppression of the condensate density scales with $-h^2$. However, this gain in SC condensation energy should be rather small, especially because the c-axis coherence length of the high-T_c superconductor is much shorter than the thickness of the YPr-123 layers. Alternative explanations could involve an induced triplet component of the SC order parameter, which enables a long-range SC proximity effect, even in half-metallic FM layers[21]. Furthermore, it is meanwhile well established that a spin-density-wave state can coexist with superconductivity in underdoped high-T_c superconductors[22], which may well provide an additional energy and length scale that must be considered in describing the competing SC and magnetic interactions. This may explain why a corresponding superconductivity-induced anomaly has not been observed yet in superlattices with optimally doped $YBa_2Cu_3O_7$ layers[12,15].

Another interesting question concerns the coupling between the structural and the magnetic domains in the LCMO layers and the question of whether it occurs on the micrometre or rather on the nanometre scale. Similar microscopic structural domains were previously observed for pure LCMO films on STO substrates[23], where transmission electron microscopy measurements also resolved nanoscale domains, which are probably related to a monoclinic phase that is induced in LCMO through the strain from the substrate[24]. We suspect that similar nanoscale domains are also present in the LCMO layers of our superlattice and are primarily responsible for the directional dependence of the superconductivity-induced modulation. The resulting strain effects are likely sufficient to change, for example through their impact on the spin–orbit coupling and/or the Jahn–Teller distortions, the subtle energy balance that determines the magnetic domain state in the LCMO layers and consequently its competition with superconductivity in the YPr-123 layers.

A possibly related issue concerns the currently unresolved question of why the average magnetization density hardly changes below T_{sc} despite the superconductivity-induced modulation of the FM magnetization density which involves large changes in the magnetization of the individual LCMO layers. In this context, it may well be that coupled magnetic and SC domain states are playing a fundamental role. A corresponding model in terms of a spatially inhomogeneous distribution of the magnetic potentials in the LCMO layers is detailed in Supplementary Fig. S8. However, we remark that this particular model relies on the fairly unrealistic assumption that the FM order in some domains of the LCMO layers develops concurrently with the onset of SC in the adjacent regions of the YPr-123 layers. Currently we are not aware of a more realistic inhomogeneous model that can account for our reflectometry data. Nevertheless, future experiments with local probe techniques may well provide the required additional information about the relevant magnetic and electronic nanoscale domains and their superconductivity-induced changes.

Methods

Two $[Y_{0.6}Pr_{0.4}Ba_2Cu_3O_7(\alpha\ \mathrm{nm})/La_{2/3}Ca_{1/3}MnO_3\ (\alpha\ \mathrm{nm})]_{10}$ superlattices with $\alpha = 10$ and 8.5 were grown on atomically flat (001) surfaces of 0.5-mm-thick STO substrates by pulsed laser deposition using the same conditions as described in refs 9,11,12,15. The structural quality of our superlattice has been previously confirmed with several characterization methods[11,12,15,18]. Different from previously studied superlattices, the present ones contain $Y_{0.6}Pr_{0.4}Ba_2Cu_3O_7$ layers that are strongly underdoped[25] with respect to the dome-shaped phase diagram of T_{sc} versus hole concentration of the CuO_2 layers[26]. The values of $T_{sc} \approx 40$ K and $T_{\mathrm{Curie}} \approx 190$ K, and the saturation magnetization of $\mu^{\mathrm{sat}} \approx 2.4\,\mu_B$ per Mn ion of our superlattices, are only moderately suppressed as compared with the bulk materials with $T_{sc} \approx 40$–50 K (ref. 25), $T_{\mathrm{Curie}} \approx 260$ K and $\mu^{\mathrm{sat}} \approx 3.7\,\mu_B$ per Mn ion[3,4].

The specular polarized and unpolarized neutron reflectometry experiments were carried out at the AMOR and MORPHEUS beamlines of SINQ at the Paul Scherrer Institut in Villigen, Switzerland. The off-specular measurements were made at AMOR and at the ADAM beamline of the Institute Laue Langevin in Grenoble, France. In both cases the samples were clamped under uniaxial pressure on the cold finger of a closed-cycle refrigerator and an in-plane magnetic field of 0.01 T was applied with a pair of Helmholtz coils. More details on the neutron reflectometry technique can be found in refs 27,28 and in Supplementary Figs S1–S3.

The magnetization measurements were obtained with a commercial (QD-PPMS-9) vibrating-sample magnetometer. The measurements under uniaxial pressure were made with a home-made sample holder, where the sample was clamped with a spring-loaded system.

References

1. Buzdin, A. I. Proximity effects in superconductor–ferromagnet heterostructures. *Rev. Mod. Phys.* **77**, 935–976 (2005).
2. Izyumov, Yu. A., Proshin, Yu. N. & Khusainov, M. G. Competition between superconductivity and magnetism in ferromagnet/superconductor heterostructures. *Phys. Usp.* **45**, 109–148 (2002).
3. Coey, J. M. D., Viret, M. & von Molnár, S. Mixed-valence magnanites. *Adv. Phys.* **48**, 167–263 (1999).
4. Salamon, M. B. & Jaime, M. The physics of manganites: Structure and transport. *Rev. Mod. Phys.* **73**, 583–628 (2001).

5. Sen, C., Alvarez, G. & Dagotto, E. Competing ferromagnetic and charge-ordered states in models for manganites: The origin of the colossal magnetoresistance effect. *Phys. Rev. Lett.* **98**, 127202 (2007).
6. Dagotto, E., Hotta, T. & Moreo, A. Colossal magnetoresistance materials: The key role of phase separation. *Phys. Rep.* **344**, 1–153 (2001).
7. Jakob, G., Moshchalkov, V. V. & Bruynseraede, Y. Superconductivity and giant negative magnetoresistance in $YBa_2Cu_3O_7/La_{0.67}Ba_{0.3}3MnO_3$ superlattices. *Appl. Phys. Lett.* **66**, 2564–2566 (1995).
8. Przyslupski, P., Kolesnik, S., Dynowska, E., Skoskievicz, T. & Sawicki, M. Fabrication and properties of $YBa_2Cu_3O_7/RE_{(1-x)}A_{(x)}MnO_{(3-y)}$ multilayers. *IEEE Trans. Appl. Supercond.* **7**, 2192–2195 (1997).
9. Habermeier, H. U. *et al.* Cuprate/manganite superlattices—a model system for a bulk ferromagnetic superconductor. *Physica C* **364/365**, 298–304 (2001).
10. Sefrioui, Z. *et al.* Ferromagnetic/superconducting proximity effect in $La_{0.7}Ca_{0.3}MnO_3/YBa_2Cu_3O_{7-\delta}$ superlattices. *Phys. Rev. B* **67**, 214511 (2003).
11. Holden, T. *et al.* Proximity induced metal–insulator transition in $YBa_2Cu_3O_7/La_{2/3}Ca_{1/3}MnO_3$ superlattices. *Phys. Rev. B* **69**, 064505 (2004).
12. Stahn, J. *et al.* Magnetic proximity effect in perovskite superconductor/ferromagnet multilayers. *Phys. Rev. B* **71**, 140509(R) (2005).
13. Peña, V. *et al.* Giant magnetoresistance in ferromagnet/superconductor superlattices. *Phys. Rev. Lett.* **94**, 057002 (2005).
14. Hoffmann, A. *et al.* Suppressed magnetization in $La_{0.7}Ca_{0.3}MnO_3/YBa_2Cu_3O_{7-\delta}$ superlattices. *Phys. Rev. B.* **72**, 140407(R) (2005).
15. Chakhalian, J. *et al.* Magnetism at the interface between ferromagnetic and superconducting oxides. *Nature Phys.* **2**, 244–248 (2006).
16. Bulaevskii, L. N., Buzdin, A. I., Kulić, M. L. & Panjukov, S. V. Coexistence of superconductivity and magnetism theoretical predictions and experimental results. *Adv. Phys.* **34**, 175–261 (1985).
17. Tokura, Y. & Tomioka, Y. Colossal magnetoresistive manganites. *J. Magn. Magn. Mater.* **200**, 1–23 (1999).
18. Hoppler, J. *et al.* X-ray study of structural domains in the near-surface region of $SrTiO_3$ substrates with $Y_{0.6}Pr_{0.4}Ba_2Cu_3O_7/La_{2/3}Ca_{1/3}MnO_3$ superlattice grown on top. *Phys. Rev. B* **78**, 134111 (2008).
19. Wollan, E. O. & Koehler, W. C. Neutron diffraction study of the magnetic properties of the series of perovskite-type compounds $[(1-x)La, xCa]MnO_3$. *Phys. Rev.* **100**, 545–563 (1955).
20. Baladie, I. & Buzdin, A. I. Thermodynamic properties of ferromagnet/superconductor/ferromagnet nanostructures. *Phys. Rev. B.* **67**, 014523 (2003).
21. Pena, V. *et al.* Coupling of superconductors through a half-metallic ferromagnet: Evidence for a long-range proximity effect. *Phys. Rev. B* **69**, 224502 (2004).
22. Lake, B. *et al.* Antiferromagnetic order induced by an applied magnetic field in a high-temperature superconductor. *Nature* **415**, 299–302 (2002).
23. Vlasko-Vlasov, V. K. *et al.* Direct magneto-optical observation of a structural phase transition in thin films of manganites. *Phys. Rev. Lett.* **84**, 2239–2242 (2000).
24. Lebedev, O. I., Van Tendelo, G., Amelinckx, S., Leibold, B. & Habermeier, H.-U. Structure and microstructure of $La_{1-x}Ca_xMnO_{3-\delta}$ thin films prepared by pulsed laser deposition. *Phys. Rev. B* **58**, 8065–8074 (1998).
25. Bernhard, C., Holden, T., Golnik, A., Lin, C. T. & Cardona, M. Far-infrared c-axis conductivity of flux-grown $Y_{1-x}Pr_xBa_2Cu_3O_7$ single crystals studied by spectral ellipsometry. *Phys. Rev. B* **62**, 9138–9142 (2000).
26. Tallon, J. L., Bernhard, C., Shaked, H., Hitterman, R. L. & Jorgensen, J. D. Generic superconducting phase-behaviour in high-T_c cuprates: T_c variation with hole concentration in $YBa_2Cu_3O_{7-\delta}$. *Phys. Rev. B* **51**, 12911–12914 (1995).
27. Holý, V., Pietsch, U. & Baumbach, T. *High-Resolution X-Ray Scattering from Thin Films and Multilayers* Vol. 149 (Springer Tracts in Modern Physics, Springer, 1999).
28. Daillant, J. & Gibaud, A. (eds) *X-ray and Neutron Reflectivity: Principles and Applications* (Lecture Notes in Physics m 58, Springer, 1999).

Acknowledgements

This work is based on experiments carried out at the Swiss spallation neutron source SINQ and the Swiss light source SLS at Paul Scherrer Institute, Villigen, Switzerland. Some of the measurements were also made at the neutron reactor of the Institute Laue Langevin, France. We acknowledge support from M. Wolff at the Institute Laue Langevin. We appreciate stimulating discussions with D. Baeriswyl, G. Khaliullin and A.F. Volkov. Work at the University of Fribourg was funded by the Schweizerische Nationalfonds zur Förderung der Wissenschaften through grants 200020-119784 and 206021-113057 and by the NCCR program MANEP.

Author contributions

J.H., J.S., Ch.N. and C.B. carried out the neutron experiments, J.H., J.S., Ch.N., A.D., A.B. and C.B. analysed and interpreted the data and V.M., H.B., M.R., G.C., H.H. and B.K. prepared and characterized the samples.